

Spatio-temporal evolution of the Kolumbo Volcanic Chain and its link to the volcanic plumbing system of Santorini

Jonas Preine¹, Christian Hübscher², Jens Karstens³, Gareth J Crutchley⁴, and Paraskevi Nomikou⁵

¹University of Hamburg

²Universität Hamburg

³GEOMAR Helmholtz Centre for Ocean Research Kiel

⁴GEOMAR - Helmholtz Centre for Ocean Research Kiel

⁵University of Athens

December 7, 2022

Abstract

The Christiana-Santorini-Kolumbo volcanic field in the southern Aegean Sea is one of the most hazardous volcanic regions in the world. Forming the northeastern part of this volcanic field, the Kolumbo Volcanic Chain (KVC) comprises more than 20 submarine volcanic cones. However, due to their inaccessibility, little is known about the spatio-temporal evolution and tectonic control of these submarine volcanoes and their link to the volcanic plumbing system of Santorini. In this study, we use multichannel reflection seismic imaging to study the internal architecture of the KVC and its link to Santorini. We show that the KVC evolved during two episodes, which initiated at ~ 1 Ma with the formation of mainly effusive volcanic edifices along a NE-SW trending zone. The cones of the second episode were formed mainly by submarine explosive eruptions between 0.7 and 0.3 Ma and partly developed on top of volcanic edifices from the first episode. We identify two prominent normal faults that underlie and continue the two main trends of the KVC, indicating a direct link between tectonics and volcanism. In addition, we reveal several buried volcanic centers and a distinct volcanic ridge connecting the KVC with Santorini, suggesting a connection between the two volcanic centers in the past. This connection was interrupted by a major tectonic event and, as a result, the two volcanic systems now have separate, largely independent plumbing systems despite their proximity.

Hosted file

essoar.10512943.1.docx available at <https://authorea.com/users/536231/articles/611172-spatio-temporal-evolution-of-the-kolumbo-volcanic-chain-and-its-link-to-the-volcanic-plumbing-system-of-santorini>

Spatio-temporal evolution of the Kolumbo Volcanic Chain and its link to the volcanic plumbing system of Santorini

J. Preine¹, C. Hübscher¹, J. Karstens², G. J. Crutchley², P. Nomikou³

¹University of Hamburg, Institute of Geophysics, Hamburg, Germany

²GEOMAR – Helmholtz Zentrum für Ozeanforschung, Marine Geophysics, Kiel, Germany

³National and Kapodistrian University of Athens, Athens, Greece

Corresponding author: Jonas Preine (jonas.preine@uni-hamburg.de)

Key Points

- High-resolution reflection seismic data reveals that the internal architecture of the Kolumbo Volcanic Chain
- The Kolumbo Volcanic Chain evolved during two episodes along NE-SW striking normal faults
- A prominent volcanic ridge connects the Kolumbo Volcanic Chain with Santorini highlighting a former connection between both systems

Abstract

The Christiana-Santorini-Kolumbo volcanic field in the southern Aegean Sea is one of the most hazardous volcanic regions in the world. Forming the northeastern part of this volcanic field, the Kolumbo Volcanic Chain (KVC) comprises more than 20 submarine volcanic cones. However, due to their inaccessibility, little is known about the spatio-temporal evolution and tectonic control of these submarine volcanoes and their link to the volcanic plumbing system of Santorini. In this study, we use multichannel reflection seismic imaging to study the internal architecture of the KVC and its link to Santorini. We show that the KVC evolved during two episodes, which initiated at ~1 Ma with the formation of mainly effusive volcanic edifices along a NE-SW trending zone. The cones of the second episode were formed mainly by submarine explosive eruptions between 0.7 and 0.3 Ma and partly developed on top of volcanic edifices from the first episode. We identify two prominent normal faults that underlie and continue the two main trends of the KVC, indicating a direct link between tectonics and volcanism. In addition, we reveal several buried volcanic centers and a distinct volcanic ridge connecting the KVC with Santorini, suggesting a connection between the two volcanic centers in the past. This connection was interrupted by a major tectonic event and, as a result, the two volcanic systems now have separate, largely independent plumbing systems despite their proximity.

Plain Language Summary

In the central Aegean lies the Christiana-Santorini-Kolumbo volcanic system, one of the most volcanically and seismically active regions in Europe. Santorini

has had over 200 eruptions in the last 360,000 years. Only 7 km northeast of Santorini lies the underwater volcano Kolumbo, as well as over 20 other smaller underwater volcanoes that form the Kolumbo Volcanic Chain, which have only had 2 major eruptions during this time. In this study, we investigate the history of this volcanic system to understand its relation to Santorini and why volcanoes located so closely together behave so differently. Using seismic reflection data image the internal architecture of the Kolumbo Volcanic Chain and show that it evolved in two episodes along two prominent faults that might continue underneath Santorini. We also identify a volcanic ridge that lies between Santorini and Kolumbo, indicating a connection between the two systems. Our study suggests that Santorini and the Kolumbo Volcanic Chain evolved as one system in the geological past, but became disconnected from each other during a major tectonic event about 300,000 years ago.

1 Introduction

Violent explosive eruptions at volcanic arcs account for ~95% of all eruption-related fatalities since 1600 CE, many associated with eruptions of coastal or marine volcanoes (e.g., Krakatau, or Tambora; Auker et al., 2013; Brown et al., 2017). As recently demonstrated by the 2022 eruption of Hunga Tonga–Hunga Ha apai, seawater interaction during shallow eruptions is capable of producing violent phreatomagmatic explosions that generate ocean-scale tsunamis (Carvajal et al, 2022; Lynett et al., 2022). In arc settings, magma is generated by partial melting of the mantle above the subducting slab, and its ascent to the surface is governed by thermodynamic conditions within the crust (e.g., Cashman & Sparks, 2017). Volcanic plumbing systems represent a complex network of vertically extensive melt reservoirs at different depths, developed over long timescales during the growth of a volcano (e.g., Tibaldi & Bonali, 2017). At shallow depths, magma rises along faults and fractures influenced by the regional tectonic stress state, which can lead to the formation of volcanic lineaments (e.g., Tibaldi, 1995). Magma path orientation can be stable over long time scales but modifications in the tectonic stress regime, such as from large earthquakes or modifications in volcano morphology, can influence the volcanic plumbing system (e.g., Hill et al., 2002). This can lead to temporal changes in the eruptive style of individual volcanoes or over short distances from one volcano to another (e.g., Hill et al., 2002).

Investigating the spatio-temporal evolution of the orientation of volcanic plumbing systems is important for understanding the behavior of active volcanoes (e.g., Tibaldi & Bonali, 2017). Being hidden beneath the surface, the deep structure and temporal evolution of volcanic plumbing systems can only be assessed on the basis of geochemical constraints (e.g., Druitt et al., 2012), by studying eroded volcanoes (e.g., Tibaldi et al., 2013) or indirectly via geodetic monitoring (e.g., Bato et al., 2018). However, these methods are difficult to apply to submarine volcanoes due to their inaccessibility for direct sampling and monitoring (Carey & Sigurdsson, 2007; Mitchell 2012). Here, geophysical methods are required, and recent advances in seismic tomography and full-waveform

inversion enable the imaging of shallow melt reservoirs underneath active volcanoes (e.g., Paulatto et al., 2022), but often lack the resolution required to reconstruct the temporal evolution of the system. This critical observational gap can be addressed by high-resolution multichannel seismic imaging, which provides structural images of the subsurface that can be used to reconstruct the relative spatio-temporal evolution of submarine volcanic systems (e.g., Preine et al., 2022a).

One of the few areas worldwide, where crustal-scale and high-resolution geophysical data as well as detailed petrological analyses are available, is the Christiana-Santorini-Kolumbo (CSK) volcanic field in the southern Aegean Sea (Fig. 1) (Nomikou et al., 2019). This 60-km-long volcanic field has produced over 200 eruptions in the last 360 thousand years, including the famous Minoan eruption of Santorini 1600 BCE (e.g., Druitt et al., 1999; Nomikou et al., 2016a; Satow et al., 2021). Located only 7 km northeast of Santorini lies the submarine Kolumbo volcano, which last erupted in 1650 CE, causing ~70 fatalities on Santorini and generated a tsunami that inundated the nearby Cycladic islands (Fouque, 1879; Cantner et al., 2014; Karstens et al., In Review_A). This eruption created a 500 m deep and 1500 m wide crater, which hosts an active hydrothermal vent field (Carey et al., 2011; 2013; Fuller et al., 2018). Kolumbo consists of five vertically stacked volcanic units (Hübscher et al., 2015) and is the largest volcano of the Kolumbo Volcanic Chain (KVC), which itself consists of more than 20 submarine volcanoes that are aligned along two NE-SW striking lineaments 16 km northeast of Kolumbo (Nomikou et al., 2012; Hooft et al., 2017).

Since the entire CSK field lies in the same regional rift system, it is subject to a common external tectonic control (e.g., Heath et al., 2019; 2021; Preine et al., 2022c). There is an ongoing discussion regarding the role of regional (> 10 km length) and local (< 10 km length) faults on the emplacement of volcanic features (Hübscher et al., 2015; Heath et al., 2021) and regarding the connection of the plumbing system between the different volcanic centers. While geochemical analyses of the eruption products from both volcanoes suggest independent crustal differentiation (Klaver et al., 2016; Risso et al., 2016), seismic tomography showed the presence of a low-velocity anomaly connecting Santorini and Kolumbo at a depth of 3-5 km, interpreted as a zone of magmatic intrusions (Heath et al., 2019; McVey et al., 2020). To date, it is not clear whether there is further evidence for a link between the Santorini volcanic system and the Kolumbo Volcanic Chain, nor is it known how their plumbing systems have evolved in time and space. To address these questions, in this study we investigate the internal architecture of the volcanic edifices from the KVC and explore their relationship to the regional tectonic system using seismic reflection images. Furthermore, we investigate seismic reflection evidence for volcanic features in the area between Santorini and Kolumbo. Based on these analyses, our objectives are to (1) reconstruct the spatio-temporal evolution of the Kolumbo Volcanic Chain, and (2) investigate whether there is a link between the evolution of Santorini and the Kolumbo Volcanic Chain.

2 Geological Framework

The KVC is part of the CSK volcanic field, one of the most active volcanotectonic regions in the Mediterranean Sea (e.g. Bohnhoff et al., 2006; Nomikou et al., 2019). Formed by the partial melting of the subducting African slab beneath the Eurasian plate, volcanism along the CSK field evolved in four phases, which initiated in the Late Pliocene with the emergence of the Christiana Volcano southwest of present-day Santorini (Phase 1; Piper et al., 2007; Preine et al., 2022a). The subsequent formation of major NE-SW trending fault systems in Middle Pleistocene correlates with the emergence of the early Kolumbo and Poseidon centers (Phase 2), which deposited volcanoclastic material in the Christiana and Anhydros Basins, respectively (Hübscher et al., 2015; Preine et al., 2022a; 2022c). The KVC is thought to have formed after a major tectonic pulse that triggered a cascade of large-scale mass-wasting events at Santorini and Kolumbo (Phase 3; Preine et al., 2022b; 2022c). This series of events marks the beginning of the third phase, which is thought to include not only the formation of the KVC, but also buried volcanic cones southwest of Santorini, and the evolution of the onshore exposed Akrotiri rhyolitic center, the Peristeria stratovolcano, and the Akrotiri cinder cones (Druitt et al., 1999; Preine et al., 2022a). In the last phase (since ~360 ka; Phase 4), a major tectonic event occurred in the Santorini-Anafi Basin, followed by the onset of highly explosive volcanism at Santorini, which corresponds to a distinct change in the primitive melt diversity (Flaherty et al., 2022). This explosive volcanism formed the Thera Pyroclastic Formation, while Kolumbo remained active producing two major eruptions (Preine et al., 2022a, 2022c).

Kolumbo's five units (K1-K5) formed over the course of more than 1 million years (Hübscher et al., 2015; Preine et al., 2022a). Seismic reflection data have shown that these volcanic units generally have low-amplitude internal reflections, indicating that they were formed by explosive underwater eruptions (Hübscher et al., 2015). This is consistent with ROV surveys of the crater walls, which show they consist of over 250 m of pumice lapilli and pumice block breccias produced by the historic 1650 CE eruption (Carey et al., 2011). Presently, a hydrothermal vent field is still active in the northern part of the Kolumbo crater (Carey et al., 2011; 2013), and frequent swarms of microseismicity indicate ongoing melt ascent (Schmid et al., 2022) from a melt reservoir at ~2 to 4 km below the crater (Chrapkiewicz et al., 2022).

Northeast of Kolumbo, volcanoes within the KVC occur in water depths of up to 450 m, with summit heights of up to 200 m above the surrounding seafloor (Nomikou et al., 2012). Most of these volcanoes are cone-shaped, with some having characteristic craters at the top, while most have smooth, rounded summits (Fig. 1c) (Nomikou et al., 2012; Hooft et al., 2017). The cones of the KVC are aligned along two main trends that are approximately linear and NE-SW oriented (orange dotted lines in Fig. 1d), lying parallel to the main fault trend of the CSK rift zone (Nomikou et al., 2012; Hübscher et al., 2015). Only two volcanoes (VC8 and VC16) lie off these main lineaments (Fig. 1c). ROV surveys

revealed that the volcanoes are sediment-covered and show little to no evidence of recent volcanic activity (Nomikou et al., 2012). Volcanic rock outcrops on the cones consist of fragments of pumice and lava that have been cemented by biological activity, while some show evidence of recent low-temperature hydrothermal activity (Nomikou et al., 2012). In general, the bases of the slopes consist of fine-grained material, while the upper slopes consist of pumice clasts and scattered lapilli (Nomikou et al., 2012; Carey et al., 2013). Previous seismic surveys of some of the volcanic cones revealed low-amplitude reflections within the volcanic cones, which were interpreted as volcanoclastic material from explosive eruptions similar to those that formed the Kolumbo volcano (Hübscher et al., 2015).

An important influence of the local tectonic system on the emplacement of volcanoes at the CSK field has been suggested by previous studies due to the overall linear alignment of volcanic edifices parallel to the NE-SW striking regional rift system (e.g., Druitt et al., 1999; Dimitriadis et al., 2009; Feulliet, 2013, Heath et al., 2019; 2021; Preine et al., 2022c). The two most prominent volcano-tectonic lineaments are the Kameni and Kolumbo lines, which strike NE-SW intersecting the northern part of the Santorini caldera (Fig. 1a) (Druitt et al., 1999; Heath et al., 2019; Hooft et al., 2019; McVey et al., 2020) (Fig. 1a). While the Kameni line is defined by a linear alignment of post-Minoan vents in the center of the caldera, the Kolumbo line connects older volcanic centers in the northern caldera basin and extends towards Kolumbo (Fig. 1a). Both lineaments bound a region of isolated caldera collapse (Hooft et al., 2019) as well as a low-velocity anomaly in the depth of 3 to 5 km that extends from the northern caldera basin towards Kolumbo (Heath et al., 2019; McVey et al., 2020).

3 Methods

In this study, we utilize an extensive dataset of more than 3,200 km of high-resolution multi- and single-channel seismic data acquired during six cruises between 2006 and 2019 (Fig. 1b) (Sigurdsson et al., 2006; Hübscher et al., 2006; Karstens et al., 2020). For all multichannel seismic lines, we applied multiple removal by means of surface-related multiple elimination and pre-stack time migration to improve the quality of the seismic images. More details on the acquisition and processing of the seismic data can be found in *Supplementary Information S1*. All processed seismic lines were combined into an interpretation project using the Kingdom Suite software. In Figure 4, we use instantaneous phase plots (Taner et al., 1979) to highlight low-amplitude but coherent events within the volcanic edifices.

4 Seismic interpretation

4.1 Seismo-stratigraphic framework

To establish a relative chronology of the evolution of the KVC, we use the seismo-stratigraphic framework established in Preine et al. (2022a, b). This framework consists of six units separated by six key horizons h1-h6. Unit 1 overlies the acoustic basement and consists of sub-parallel reflections of very

low amplitude, which are often difficult to image due to the overprint of the seafloor multiple. The overlying Unit 2 consists of a series of well-stratified reflections with low to medium amplitudes. Units 3 and 5 consist of a series of well-stratified medium amplitude reflections. In contrast, Unit 4 consists of chaotic, weakly reflective material that has been interpreted as the deposits of the Santorini mass wasting cascade (Preine et al., 2022b). Where Unit 4 is missing, Unit 5 directly overlies Unit 3. The uppermost Unit 6 consists of high amplitude reflections that become irregular near Santorini, where they comprise the deposits of the Thera Pyroclastic Formation (Preine et al., 2022a). For the interpretation of the volcanic units of Kolumbo, we follow the nomenclature of Hübscher et al. (2015), who labeled the Kolumbo Units K1-K5.

4.2 Kolumbo Volcano and the Kolumbo Volcanic Chain

Figure 2 shows two seismic profiles crossing the Kolumbo Volcano perpendicular to each other. The uppermost profile crosses the Anhydros Basin and Kolumbo in the NW-SE direction (Fig. 2a). In the Anhydros Basin, we identify all seismostratigraphic Units, which have relatively constant thicknesses. There are several faults intersecting the strata of the Anhydros Basins, with the Kolumbo Fault being the most prominent (as shown also in Nomikou et al., 2016b; Preine et al., 2022a). On top of the uppermost Unit U6, we identify a chaotic subunit, which thickens towards Kolumbo and represents the Minoan ignimbrites (yellow semi-transparent area) (Hübscher et al., 2015; Karstens et al., In Review_B). This Unit is overlain by Kolumbo’s Unit K5, which consists of well-stratified reflections representing the pumice deposits of the 1650 CE eruption (Cantner et al., 2014; Hübscher et al., 2015; Karstens et al., In Review_A). Kolumbo’s Unit K4 lies at the basis of Unit U6 and consists of chaotic to transparent internal reflections (Fig. 2a). K3 is comparatively small and intercalated within Unit U5, while K2 makes up most of the Kolumbo edifice and is partly exposed on the crater wall (Fig. 2b). Both K2 and K1 are intercalated within Unit U3 and separated from each other by prominent high-amplitude reflections (Fig. 2a). In the center of the Kolumbo crater, we identify an acoustically transparent structure, which represents a dyke that is exposed on the crater wall (Karstens et al., In Review_A).

The profile in Figure 2b starts on the eastern flank of Santorini, crosses the Kolumbo crater, and eight additional cones of the KVC. On the flank of Santorini, we identify the Minoan ignimbrites, which have a wavy topography typical for submarine pyroclastic flow deposits (Pope et al., 2018). Horizon h6 marks a distinct onlap surface, onto which most of the internal reflections of Unit 6 terminate (orange arrows, Fig. 2b). Unit 4 is absent in this profile and the deeper Units 1-3 are difficult to interpret since the seismic image is disturbed in the deeper part, especially below the KVC or towards Santorini (Fig. 2b). At profile kilometer 2.5, we identify a high-amplitude reflection within Unit 4 (red dashed line, Fig. 2b), causing acoustic blanking underneath, which may indicate a small volcanic edifice (Fig. 2b).

Beneath Kolumbo, we identify the Kolumbo Units K1, K2, K4, and K5. Unit

K4 is relatively small here, while K3 appears to be absent. On the southwest side of Kolumbo, the termination of K2 and K1 is well imaged (~km 5, Fig. 2b). However, the termination towards the northeast below the KVC cannot be constrained as the seismic image becomes highly disturbed below the KVC.

The cones of the KVC crossed in this profile decrease in height towards the NE and display complex onlapping relationships with each other (Fig. 2b). In general, the cones have an internal architecture similar to that of Kolumbo, consisting of stratified flanks with weak seismic amplitudes and a chaotic, weakly reflective core (Fig. 2b). The cones are located on top of weakly reflective strata with several high amplitude reflections (purple semi-transparent area, Fig. 2b). Underneath VC2 and VC6, we observe a zone of vertically pervasive blanking and velocity pull-up (marked ‘blanking’ in Fig. 2b), which is a typical effect occurring beneath high-velocity volcanic rocks within a sedimentary sequence (e.g., Jackson, 2012; Magee et al., 2013b; Reynolds et al., 2018). Beneath VC6, we observe a sequence of well-stratified reflections that onlap a cone-shaped, acoustically transparent area (orange triangles, Fig. 2b).

Figure 3 shows three seismic profiles traversing the central part of the KVC. The uppermost profile crosses the Anhydros Basin and the southwestern part of the KVC including VC6, VC5, and VC3 (Fig. 3a). In the Anhydros Basin, we identify all six seismostratigraphic units and the Ios and Kolumbo Faults to the NW of the KVC. Between the Kolumbo Fault and the KVC is a complex fault zone with several small offset internal faults that terminate within Units 3 and 4 (Fig. 3a). Southeast of the KVC, towards the Anhydros Horst, we observe additional internal faults. The flanks of the volcanic cones are all intercalated with Unit 5. There is a zone of pronounced seismic blanking and velocity pull-ups beneath the central part of VC5, while underneath VC6, we identify a zone of chaotic, low amplitude reflections (purple semi-transparent area, Fig. 3a). The reflections from Unit 5 overly and/or onlap this cone-shaped area (km 15 in Fig. 3a). It is noteworthy that the base of e.g. VC5 lies approximately 130 ms beneath the seafloor, implying that the total height of VC5 is about 115 m greater than the 200 m protruding upwards from the seabed (assuming a velocity of 1750 m/s for unit 6 and 1500 m/s as water velocity, Preine et al. (2022a)).

The seismic profile in Figure 3b crosses the Ios Fault and the deep part of the Anhydros Basin, where we find all six seismostratigraphic units and several internal faults (Fig. 3b). The profile crosses the flanks of VC5 and VC11 as well as VC7 and VC8. While VC5 and VC11 cause no pull-up or acoustic blanking indicating a moderate internal velocity of the flanks, VC7 and VC8 cause complete blanking of the underlying strata except for some scattered reflection patches (purple dashed lines, Fig. 3b). The margin of the Anhydros Basin and the Anhydros Horst is not resolved due to the acoustic blanking (Fig. 3b). Figure 3a shows that VC7 onlaps VC8, while the northwestern flank of VC7 occurs within Unit 3, suggesting an older age for these two cones compared to the other cones of the KVC, which are within Unit 5 (Preine et al., 2022a) (Fig.

3b).

The seismic profile in Figure 3c is similarly oriented to the profile crossing the Ios Fault and the Anhydros Basin. Figure 3c crosses VC16, which is slightly further west than the rest of the KVC (Figs. 1, 3c). We identify high amplitude and irregular reflections at the top of this edifice (VC16) and pronounced acoustic blanking underneath (Fig. 3c). This is in contrast to the flanks of VC5 and VC11 (Fig. 3b) or VC5 and VC6 (Fig. 3a), where the acoustic blanking is much less pronounced and we can identify reflections below the cones. On the other hand, the acoustic characteristics of VC16 are similar to those of VC7 and VC8 (Fig. 3b), where complete acoustic blanking is observed. Furthermore, Figure 3c shows that below VC12, the reflections of Unit 3 onlap a body of chaotic/transparent internal reflections, which is connected to a broad zone of pronounced acoustic blanking beneath VC9 and VC8 (purple semi-transparent area in Fig. 3b). Similar to Figure 3b, the transition from the Anhydros Basin to the Anhydros Horst is not resolved in this profile (Fig. 3c).

The profiles shown in Figures 2 and 3 highlight that the internal architecture of the different volcanic edifices of the KVC is diverse. To examine this in more detail, Figure 4 shows enlargements of selected volcanoes from the KVC with their respective instantaneous phase representations, which reveal weak coherent events within the volcanic edifices. We identify the following three main characteristic features:

Seismic Facies 1 (SF1): Many volcanic cones have well-stratified flanks with a pronounced downlap termination towards the base of the edifice (VC3, VC6, VC11, and VC12) (Fig. 4). While these reflections have low amplitudes and are barely visible in the amplitude plots (Fig. 4a, c, e), they are visible as coherent closely-spaced reflections in the instantaneous phase plots (Fig. 4b, d, f). Similar stratified flanks can be observed within Unit K5 of Kolumbo (Fig. 2a, b), where they represent stratified pumice deposits of the explosive 1650 eruption (Hübscher et al., 2015; Karstens et al. In Review_B). Based on the similarity between the stratified flanks of the volcanic cones and the internal structure of Kolumbo's unit K5, we interpret that stratified flanks of the cones are seismic indicators of pumiceous deposits and are thus indicative of explosive eruptions.

Seismic Facies 2 (SF2): All of the volcanic cones investigated in this study exhibit regions of incoherent seismic facies, which we will refer to as SF2. While SF2 is visible as acoustically blanked areas in the amplitude plots (Fig. 4a, c, e), the instantaneous phase plots show chaotic, incoherent internal reflections (Fig. 4b, d, f). We identify SF2 in the central area of the volcanic cones close to the vents (VC6, VC11) (Fig. 4), or within some of the acoustically transparent structures below the cones, e.g., below VC6 or VC12 (Fig. 6). In several instances, the incoherency of the strata cannot be explained by velocity effects from the overlying structures alone, as e.g., below VC6, individual horizons can be clearly imaged and traced underneath the volcanic cone, showing a distinct onlap behavior to the underlying incoherent region, which itself has a cone-like shape

(Fig. 4a, b). This suggests that these features are buried volcanic structures over which newer volcanic cones have developed. This is evident beneath VC12, where the flank of the buried edifice is intercalated within Unit U3 (Fig. 3c, 4e, 4f). This acoustic signature could be explained by the presence of brecciated material and massive hyaloclastites in the near-vent region of volcanic edifices, which has been identified by ROV surveys in the summit regions (Nomikou et al., 2012).

We also identify the incoherent seismic facies along broader areas, e.g., within VC8 and VC16 (Fig. 6), where chaotic or acoustic blanking facies extend laterally over an area > 1 km. Below these edifices, there is complete seismic blanking and no coherent reflections can be identified in either the amplitude plot or the instantaneous frequency plot. This is in contrast to other volcanoes of the KVC (e.g., VC3, VC6, and VC12) (Fig. 6), where reflections can be identified over wide areas, also below the edifices, suggesting that VC8 and VC16 consist of a different, denser material, e.g. lava flows.

High amplitude reflection (HAR): We identify several reflections with anomalously high amplitudes compared to background reflectivity in the vicinity of several volcanic cones, e.g. next to VC11 (Fig. 4c-f), or at VC16 (Fig. 4e, f). Some of these reflections, occurring directly beneath volcanic cones, are saucer-shaped and phase-reversed and could be interpreted as sill intrusions (e.g., Planke et al., 2006; Magee et al., 2016) (e.g., Figs. 4e, f). High-amplitude reflections without phase reversals occur e.g. at VC11 directly below the crater (Fig. 4a, b), or at VC16 directly above the acoustically blanked area (Fig. 4e, f) and could be related to the presence of effusive lava flows as mentioned above.

4.3 The northeastern section of the Kolumbo Volcanic Chain

Figure 5 shows five profiles crossing the northeastern KVC and the transition to the non-volcanic eastern Anhydros Basin. In all of these profiles, we identify three major normal fault systems Ab1-Ab3, which all dip towards the southeast. The seismic profile shown in Figure 5a crosses VC17 and VC18, two of the easternmost cones of the KVC. Northwest of these volcanoes, we identify a broad zone of strong acoustic blanking that appears to be associated with the northeastern flank of VC16 (Fig. 5a). This acoustic blanking zone is overlain by Units 4-6, which appear to be uplifted (Fig. 5a). While the thickness of Unit 5 above this zone is constant, Unit 6 is very thin, suggesting that the uplift occurred prior to the deposition of Unit 6. Several faults are visible on the southeastern margin of the Anhydros Basin, including the two prominent faults Ab1 and Ab2, which can be traced along several profiles. Fault Ab1 offsets the seafloor, while Fault Ab2 shows a major throw offsetting the acoustic basement by up to 150 meters, which is also visible in the seismic profiles in Figures 5b and 5c. The volcanic edifices VC17 and VC18 appear to be located in a zone with several faults that might continue underneath these cones, although these could also be the result of acoustic disturbance due to the overlying volcanic cones (dashed lines and question marks, Fig. 5c). This is also the case in the seismic profile in Figure 5b crossing VC18, which seems to be located above several

faults (dashed lines and question marks, Fig. 5b). VC20, which is imaged in the seismic profile in Figure 5c, is located further to the NE and we identify Fault Ab2 directly below the edifice, indicating a major structural relationship between the fault and the edifice (Fig. 5c).

Overall, the sediment thickness in the profiles in Figures 5a-d decreases towards the northeast, and only Units 3-6 are visible in the profile in Figure 5e, which is also devoid of volcanic structures. We identify Fault Ab2 and Ab3 in the center of the basin, and towards Fault Ab2, the internal reflections of Unit 3 are divergent (Fig. 5d). The seismic profile in Figure 5e crosses the eastern Anhydros Basin, which represents a typical half-graben. The internal reflections of Units 2-4 thicken significantly towards the basin-bounding Ios Fault (Fig. 5e). We identify Faults Ab1 and Ab2 in the central and eastern part of the Anhydros Basin, while Fault Ab3 appears to be absent here.

4.4 The area between Kolumbo and Santorini

Figure 6 shows three seismic profiles traversing the Anhydros Basin between Kolumbo and Santorini. The first profile extends from the northeastern flank of Santorini, crossing Kolumbo and the Anhydros Horst (Fig. 6a). Similar to the profiles in Figure 2, we identify the Minoan deposits on the flank of Santorini (semi-transparent yellow color; Fig. 6a). At profile kilometer 10, there is a cone-shaped area of acoustic blanking (labeled 'Oia cone' in Fig. 6a). The internal reflections of Unit 6 onlap this feature and, since we observe a velocity pull-up beneath, we interpret this feature as a small buried volcanic cone similar to the Aspronisi cones southwest of Santorini (Preine et al., 2022a). Continuing towards Kolumbo (at km 12), we observe a high amplitude reflection with acoustic blanking beneath, at the boundary between Units 3 and 4 (red dashed lines, Fig. 6a). This feature is very similar to the feature observed on the flank of Santorini in Figure 2b. At Kolumbo, we identify all five Kolumbo Units and K3 represents a well-defined volcanic cone within Unit 5. It is noteworthy that the summit of K3 is located about 3 km away from the crater of Kolumbo and there is pronounced acoustic blanking below the center of the cone (km 15 in Fig. 6a).

Figures 6b and 6c show two profiles that are located further to the southwest, traversing the area between Kolumbo and the northeast flank of Santorini. The profiles cross the Kolumbo Ridge, which is a previously unrecognized morphological feature that extends for 6 km from the northeastern flank of Santorini towards Kolumbo (Fig. 1c). Compared to the other profiles, the strata here are more irregular, which is why some of the key horizons are indicated by dashed lines (Figs. 6b, c). In both profiles, we identify the Minoan eruption deposits as the shallowest subunit (Figs. 6b, c). The center of both profiles is dominated by a broad zone of pronounced acoustic blanking (semi-transparent purple area) and upwardly bent reflections with some scattered high amplitude reflections (marked by dashed purple lines in Figs. 6b, c). While the lower units U1-U3 cannot be traced along these zones of strong acoustic blanking, the upper units appear to partially overlie the zone of acoustic disturbance, although it is diffi-

cult to trace reflections along these zones. Only for the reflections of Unit 6 can we identify some onlap terminations towards horizon h6.

5 Discussion

5.1 Spatio-temporal evolution of the Kolumbo Volcanic Chain

Using our seismo-stratigraphic framework, we are able to establish a relative spatio-temporal model for the KVC. While the intercalation of the flanks of volcanic cones within the seismo-stratigraphic units allows us to place them in the general stratigraphic framework of the CSK field from Preine et al. (2022a), onlap terminations of individual cones against each other allow us to place them into a relative age context as summarized in Figure 7a. For example, the following relative age trend (becoming younger left to right) can be determined from onlap terminations identified in the seismic profile in Figure 2b: VC2>VC4>VC6>VC3 (Fig. 7a). However, this approach is limited to cones where our seismic data allow us to identify direct onlap terminations. Volcanic edifices that are not imaged by our data or that are too far away from each other cannot be integrated into this relative chronological framework, since internal reflections cannot be reliably traced along the often chaotic or discontinuous intra-volcanic areas.

Our analysis shows that the evolution of the KVC is much more complex than previously thought (Fig. 7a). According to the age model from Preine et al. (2022a), the Kolumbo cones evolved in a single phase during the deposition of Unit 5 and are thus between approximately 0.7 and 0.36 Myrs old (phase 3). However, Figure 3b clearly shows that VC7 and VC8 occur within Unit 3 and thus evolved during the same phase as K1 and K2 from Kolumbo, implying an age of approximately 1 Myrs (Preine et al., 2022a). The buried edifices, e.g., below VC6 and VC12 (Fig. 3a, e) also appear to have developed during this older phase indicating volcanism was widespread at that time. In addition, our seismic images show that the internal architecture of these early volcanic edifices is mainly composed of the incoherent seismic facies SF2 and that there is strong acoustic blanking underneath, which is particularly evident at VC8 (Figs. 3b, 3c, 5c, 5d). As mentioned above, this implies that the edifices from this phase are composed of a very dense, acoustically attenuating material, that could be explained by the presence of thick effusive lava flows. This is in contrast to most of the volcanoes of the younger phase, which were formed during the deposition of Unit 5 (~0.7-0.35 Ma) (Fig. 7a) and appear to have been formed primarily by explosive submarine volcanism, as indicated by the seismically well-imaged flanks (Fig. 4) that are very similar to the pumice-bearing crater walls of Kolumbo (Carey et al., 2011).

Onlap terminations from several cones of the KVC allow us to establish a relative chronological model of the evolution of the KVC (Fig. 7a) and the spatial dimension of onlap terminations is indicated in Figure 7b. However, not all volcanoes of this phase seem to have been formed by explosive eruptions, since the seismic image of VC16 is more indicative of effusive volcanism due to the

strong acoustic attenuation below and the irregular high-amplitude reflections above (Figure 3c, 4e, 4f). The seismic profile in Figure 3c suggests that Unit 6 and parts of Unit 5 lie above VC16. This is also corroborated by Figure 6a, where we interpret the acoustically disturbed zone to be an intrusion related to VC16. Here, large parts of Units 4 and 5 appear to be uplifted, with the lack of thickness variation of these units suggesting that this uplift occurred after their deposition (Fig. 6a). In contrast, Unit 6 has a much lower thickness above this area, suggesting that it was deposited after the evolution of VC16 (Fig. 6a). Thus, our analysis suggests that VC16 was formed during the deposition of Unit 5 and therefore belongs to Phase 3 of Preine et al. (2022a) (Fig. 7a), which, accordingly, saw more diverse volcanism than the formation of monogenetic cones only. Figure 7c shows a conceptual cross-section through the central part of the KVC, highlighting the different types of volcanic edifices from the two episodes of KVC evolution. The early phase saw the formation of the mainly effusive volcanic edifices such as VC8 and the buried edifices such as those found underneath VC6. The second phase saw the explosive submarine eruptions forming most of the cones of the KVC, in addition to the effusive formation of VC16, which lies off the main trend of the KVC.

5.2 The role of tectonics

The Kolumbo Chain forms two main trends that lie parallel to the NE-SW striking direction of the basin bounding faults of the Santorini-Amorgos Tectonic Zone (e.g. Nomikou et al., 2018). Hübscher et al. (2015) related these two trends with two faults that occur in the eastern Anhydros Basin. According to our study, the eastern fault trend is linked to an internal fault zone in the Anhydros Basin, while the western fault trend is connected to the Ios Fault in the Anhydros Basin, implying a direct tectonic control of the KVC. In contrast, a recent study based on seismic anisotropy along the Anhydros Basin concluded that magmatism is not localized in areas of higher fault density, but influenced by the regional-scale tectonic regime (Heath et al., 2021).

The seismic profiles shown in Figure 5 indicate that two prominent faults extend the two trends of the KVC towards the northeast into the eastern Anhydros Basin. Fault Ab2 shows a significant throw, offsetting the basement reflection by up to 150 m (Fig. 5a-c). This fault can be clearly identified directly underneath VC20, as visible in Figure 5c, and seems to continue the strike of the southeastern trend of the KVC far into the Anhydros Basin, where it is expressed as a complex system of intra-basin faults (Fig. 5e), in agreement with Hübscher et al. (2015). Fault Ab3 seems to continue the strike of the northwestern trend of the KVC and seems to continue underneath the volcanic cones VC17 and VC18 (Fig. 5a, b). However, due to the acoustic disturbances underneath the other cones, we cannot reliably trace faults Ab2 and Ab3 further underneath the KVC. On the other hand, the spatial trend of these faults (Fig. 5f) strongly indicates that these faults had an important influence on the volcanic plumbing system of the KVC, with volcanoes evolving both above and in between these faults (Fig. 5). Onlap terminations of the volcanic cones do not indicate that one of the two

trends is younger than the other, since, as can be seen in Figure 7b, there are onlap terminations between individual cones of both trends, indicating that no clear spatial age trend can be derived. Thus, the formation of the KVC appears to have occurred as a phase of widespread volcanism along both trends of the KVC (Fig. 7b).

Figure 5 also indicates that the throw of faults Ab2 and Ab3 decreases towards Unit 6, indicating that the main active phase of these faults was the time when Units 3-5 were deposited. This is particularly evident in Figure 5d, where Units 4 and 5 show significant divergence towards Fault Ab2. This is consistent with the temporal concept presented in Figure 7a, which indicates that the KVC was formed during the deposition of Units 3 and 5. Thus, in addition to the spatial aspect, this also suggests a temporal volcano-tectonic control of the KVC, i.e. that the timing of faulting corresponds to the evolution of the cones along the KVC.

5.3 Link between the Kolumbo Volcanic Chain and the plumbing system of Santorini

Our analysis has shown that the spatio-temporal evolution of the KVC is complex, including both explosive and effusive volcanism over long timescales. This raises the question of how these different phases are related to the volcanic plumbing system of Santorini. While the overprint of the thick Thera Pyroclastic Formation and several caldera collapse events complicate the analysis of the early evolution of Santorini, our seismic data allow the region between Santorini and Kolumbo to be imaged, where the Kolumbo Ridge connects the northeastern flank of Santorini with Kolumbo (Fig. 1c).

The seismic profiles in Figures 6b and 6c illuminate the internal architecture of the Kolumbo Ridge, revealing a zone of acoustic blanking with some scattered high-amplitude reflections beneath, indicating the presence of stacked volcanic edifices or widespread intrusions. The location of the Kolumbo Ridge is consistent with the low-velocity zone from McVey et al. (2020) that extends from Santorini to Kolumbo at 3.5 km depth, which they interpreted as a zone of extensive magmatic intrusions. Figure 8a shows the spatial extent of the zone of acoustic blanking underneath the Kolumbo Ridge and the KVC, which has a similar orientation to the deep low-velocity zone of McVey et al. (2020), and its boundaries coincide with the trend of the Kameni and Kolumbo Lines (Fig. 8a). Although we cannot trace faults Ab2 and Ab3 underneath the KVC and the Kolumbo Ridge, their orientation also broadly matches the trend of the Kameni and Kolumbo Lines (Heath et al., 2019) suggesting a major volcano-tectonic zone connecting Santorini, the Kolumbo ridge, and the KVC. Onshore geological mapping shows the existence of several NE-SW striking faults as well as numerous dykes on the northeastern flank of Santorini, which could represent the shallowest expression of this large-scale fault zone (e.g., Druitt et al., 1999; Drymoni et al., 2022).

In addition to the Kolumbo Ridge, our seismic data also reveal several smaller

volcanic edifices in the area between Santorini and Kolumbo. The seismic profile in Fig. 4a shows that the cone forming Kolumbo’s Unit K3 had a separate vent located several kilometers southwest of the present-day crater (area of strong acoustic blanking in Fig. 6a). We also detect some smaller volcanic features in the area between Santorini and Kolumbo, such as the Oia Cone (Fig. 4a) or smaller zones of acoustic blanking, which may be related to shallow intrusions or smaller extrusions (Figs. 2a, 4b, 8). This shows that the area between Santorini and Kolumbo has been volcanically active in the past. Considering that volcanic edifices from Phases 2 and 3 have also been identified southwest of Santorini, such as the Poseidon center and the Aspronisi cones (Preine et al., 2022a), this shows that volcanism in the CSK field was much more widespread in previous phases (Fig. 8a). This is supported by recent findings of Pank et al. (2022), who sampled submarine lava outcrops in the Santorini caldera and found several samples with ages of ~ 255 ka and $\sim 309 \pm 30$ ka (for location, see Pank et al., (2022) and Fig. 8a). These samples fill an age gap in the volcanic history of Santorini, as the transition between Peristeria volcanism (550-450 ka) and the onset of the first eruptive cycle is not well constrained (Pank et al., 2022). These authors further show that these samples have a similar Sr-N-Pb isotopic composition to the Peristeria volcano, but argue that the samples belong to a previously unknown stage of Santorini volcanism. Considering the low accuracy of absolute age estimates from seismic stratigraphy, the boundary between phases 3 and 4 (~ 360 ka) as defined in Preine et al. (2022a) has a considerable error margin. So far, the age model is based on the sedimentation rate extrapolations and the correlation to the onset of the first eruptive cycle on Santorini, which is based on tentative ages for Cape Therma 1 and Cape Therma 2 from Vakhrameeva et al. (2018, 2019) (Pank et al., 2022). Thus, it is plausible that the lavas of Pank et al. (2022) belong to Phase 3 and thus correspond to the continuation of the widespread volcanism of phase 3, which was subsequently masked by the TPF volcanism and multiple caldera collapses.

Our reconstruction of the spatio-temporal evolution of the KVC in the context of the entire CSK volcanic field and the surrounding tectonic system is illustrated in Figure 8b-e. According to this model, after volcanism initiated in Late Pliocene/Early Pleistocene with the emergence of the large Christiana edifice (Phase 1, Fig. 8b), it became widespread in the Middle Pleistocene, forming volcanic centers southwest and northeast of present-day Santorini including the first episode of the KVC (Phase 2, Fig. 8c). During this period, the tectonic system started to form prominent NE-SW striking faults, including faults Ab2 and Ab3, which appear to have strongly influenced the emplacement of volcanic edifices during this phase (Fig. 8d). After a regional tectonic pulse affected the entire CSK rift system and a major mass-wasting cascade occurred at proto-Santorini (Preine et al., 2022b), another episode of wide-spread volcanism took place, which included the onshore exposed Akrotiri and Peristeria centers, the Aspronisi cones SW of Santorini, the newly-discovered Oia Cone between Kolumbo and Santorini, as well as large parts of the younger KVC (Fig. 8d). This widespread volcanism, which occurred along a large SW-NE oriented

region, suggests that the volcanic plumbing system of the different edifices was laterally connected over a wide area, for example through long dykes systems that are typical for lateral connections along rift systems (e.g. Bato et al., 2018).

The transition from Phase 3 to Phase 4 is marked by another major rifting event, which affected predominantly the northeastern Santorini-Anafi Basin (Fig. 1b) (Preine et al., 2022c). This tectonic event had a major influence on the volcanic plumbing system of the KVC since, afterward, volcanism became more spatially isolated and explosive, focusing mainly on the northern caldera basin of Santorini (forming the TPF) and Kolumbo, which had two major eruptions including the 1650 CE K5 eruption (Preine et al., 2022c). This tectonic pulse also corresponds to a change in melt diversity of the eruptive products of Santorini (Flaherty et al., 2022). We argue that the large-scale tectonic event marking the transition from Phase 3 to Phase 4 might have interrupted the connection of the volcanic systems of Santorini and Kolumbo, which seem to have been connected during Phase 3. This could have led to a focusing of volcanic activity on distinct centers during Phase 4. This would explain why there is geophysical evidence for both a deep (McVey et al., 2020) and a shallow (this study) connection between Santorini and the KVC from previous phases, while geochemical analyses of the eruptive products show clear differences between the two systems (Klaver et al., 2016; Risso et al., 2016).

6 Conclusions

In this study, we have used reflection seismic profiles to reconstruct the spatio-temporal evolution of the Kolumbo Volcanic Chain (KVC) and its relationship to the Santorini volcanic system. We show that the KVC evolved in two main episodes. The first episode occurred at approximately 1 Ma and formed volcanic edifices along a broad NE-SW trending zone northeast of Santorini. While most cones of the volcanic edifices of this episode are buried, some have only a thin sedimentary cover or are exposed at the seafloor. These cones seem to have been formed mainly by effusive eruptions, forming thick layers of acoustic blanking in the seismic data. In contrast, volcanoes of the second episode were formed mainly during submarine explosive eruptions between about 0.7 and 0.3 Ma and formed well-stratified pumice cones that generally cause only minimal acoustic disturbances below, although at least one of these younger cones also likely formed during effusive eruptions.

We show that the two main trends of the KVC correspond to two faults that continue towards the eastern Anhydros Basin. Most of the cones formed either on top of or between these faults, indicating a pronounced influence of local tectonism on the volcanic evolution of the KVC. We also identify several buried volcanic centers in the area between Santorini and Kolumbo, as well as a broad zone of acoustic blanking connecting Kolumbo with the northeastern flank of Santorini, which we interpret as a zone of widespread volcanic intrusions. This suggests that volcanism was much more widespread in the early evolution of Santorini, and occurred along a broad NE-SW trending zone that probably continued further beneath present-day Santorini. At some point, a major tectonic

event disconnected these systems, explaining the distinct geochemical signatures of the recent eruptive products of Kolumbo and Santorini.

Our study highlights that high-resolution seismic imaging is a versatile tool for studying submarine volcanoes that are difficult to access otherwise. We show that seismic imaging can reveal buried volcanic structures, which would otherwise remain unrecognized, and allows the evolution of volcanic plumbing systems in space and time to be reconstructed. Similar high-resolution seismic surveys at the neighboring volcanic centers of the Hellenic Arc would provide a much clearer picture of the volcanic evolution and tectonic controls of this back-arc system, which is important for a more reliable hazard assessment of the region.

Data availability statement:

SEG-Y files of the seismic lines shown in Figure 2-6 are submitted to the Marine Geoscience Data System and will be publically accessible soon. Link and data DOI will be updated during the revision process.

Acknowledgments

We would like to thank the captains, crews, and scientific parties of RV Poseidon POS338 and RV Aegeo THERA expeditions. We thankfully acknowledge the support of the German Research Foundation DFG (HU690/25-1). In addition, we are grateful to Schlumberger for providing VISTA seismic processing software and IHS Markit for providing KINGDOM seismic interpretation software.

References

- Bato, M. G., Pinel, V., Yan, Y., Jouanne, F., & Vandemeulebrouck, J. (2018). Possible deep connection between volcanic systems evidenced by sequential assimilation of geodetic data. *Scientific reports*, 8(1), 1-13 <https://doi.org/10.1038/s41598-018-29811-x>
- Bohnhoff, M., Rische, M., Meier, T., Becker, D., Stavrakakis, G., & Harjes, H. P. (2006). Microseismic activity in the Hellenic Volcanic Arc, Greece, with emphasis on the seismotectonic setting of the Santorini–Amorgos zone. *Tectonophysics*, 423(1-4), 17-33, <https://doi.org/10.1016/j.tecto.2006.03.024>
- Brown, S. K., Jenkins, S. F., Sparks, R. S. J., Odbert, H., & Auker, M. R. (2017). Volcanic fatalities database: analysis of volcanic threat with distance and victim classification. *Journal of Applied Volcanology*, 6(1), 1-20, <https://doi.org/10.1186/s13617-017-0067-4>
- Chrapkiewicz, K., Paulatto, M., Heath, B. A., Hooft, E. E. E., Nomikou, P., Papazachos, C. B., ... & Morgan, J. V. Magma chamber detected beneath an arc volcano with full-waveform inversion of active-source seismic data. *Geochemistry, Geophysics, Geosystems*, e2022GC010475, <https://doi.org/10.1029/2022GC010475>
- Cantner, K., Carey, S., & Nomikou, P. (2014). Integrated volcanologic

and petrologic analysis of the 1650 AD eruption of Kolumbo submarine volcano, Greece. *Journal of Volcanology and Geothermal Research*, 269, 28-43, <https://doi.org/10.1016/j.jvolgeores.2013.10.004>

Cassidy, M., & Mani, L. (2022). Huge volcanic eruptions: Time to prepare, doi: <https://doi.org/10.1038/d41586-022-02177-x>

Carey, S., & Sigurdsson, H. (2007). Exploring submarine arc volcanoes. *Oceanography*, 20(4), 80-89, <https://doi.org/10.5670/oceanog.2007.08>

Carey, S., Bell, K. L. C., Nomikou, P., Vougioukalakis, G., Roman, C. N., Cantner, K., ... & Martin, J. F. (2011). Exploration of the Kolumbo volcanic rift zone, <https://doi.org/10.5670/oceanog.24.1.supplement>

Carey, S., Nomikou, P., Bell, K. C., Lilley, M., Lupton, J., Roman, C., ... & Ballard, R. (2013). CO₂ degassing from hydrothermal vents at Kolumbo submarine volcano, Greece, and the accumulation of acidic crater water. *Geology*, 41(9), 1035-1038, <https://doi.org/10.1130/G34286.1>

Carvajal, M., Sepúlveda, I., Gubler, A., & Garreaud, R. (2022). Worldwide signature of the 2022 Tonga volcanic tsunami. *Geophysical Research Letters*, 49(6), e2022GL098153, <https://doi.org/10.1029/2022GL098153>

Cashman, K. V., & Fiske, R. S. (1991). Fallout of pyroclastic debris from submarine volcanic eruptions. *Science*, 253(5017), 275-280, <https://doi.org/10.1126/science.253.5017.275>

Cashman, K. V., & Sparks, R. S. J. (2013). How volcanoes work: A 25 year perspective. *Bulletin*, 125(5-6), 664-690. <https://doi.org/10.1130/B30720.1>

Cronin, S., Brenna, M., Kula, T., Ukstins, I., Adams, D., Wu, J., ... & Gravley, D. (2022). The 15 January 2022 Hunga eruption, Tonga—first petrographic and geochemical results (No. EGU22-13584). *Copernicus Meetings*, <https://doi.org/10.5194/egusphere-egu22-13584>

Dimitriadis, I., Karagianni, E., Panagiotopoulos, D., Papazachos, C., Hatzidimitriou, P., Bohnhoff, M., ... & Meier, T. (2009). Seismicity and active tectonics at Coloumbo Reef (Aegean Sea, Greece): Monitoring an active volcano at Santorini Volcanic Center using a temporary seismic network. *Tectonophysics*, 465(1-4), 136-149, <https://doi.org/10.1016/j.tecto.2008.11.005>

Druitt, T. H., Edwards, L., Mellors, R. M., Pyle, D. M., Sparks, R. S. J., Lanphere, M., ... & Barreirio, B. (1999). Santorini volcano. *Geological Society Memoir*, 19

Druitt, T. H., Costa, F., Deloule, E., Dungan, M., & Scaillet, B. (2012). Decadal to monthly timescales of magma transfer and reservoir growth at a caldera volcano. *Nature*, 482(7383), 77-80, <https://doi.org/10.1038/nature10706>

Drymoni, K., Browning, J., & Gudmundsson, A. (2022). Spatial and temporal volcanotectonic evolution of Santorini volcano, Greece. *Bulletin of Volcanology*, 84(6), 1-18, <https://doi.org/10.1007/s00445-022-01566-4>

- Feuillet, N. (2013). The 2011–2012 unrest at Santorini rift: Stress interaction between active faulting and volcanism. *Geophysical Research Letters*, 40(14), 3532-3537, <https://doi.org/10.1002/grl.50516>
- Flaherty, T., Druitt, T. H., Francalanci, L., Schiano, P., & Sigmarsson, O. (2022). Temporal variations in the diversity of primitive melts supplied to the Santorini silicic magmatic system and links to lithospheric stresses. *Contributions to Mineralogy and Petrology*, 177, 79. <https://doi.org/10.1007/s00410-022-01941-6>
- Fouque, F., 1879, Santorin et ses Eruptions: Paris, G. Masson,
- Fuller, S., Carey, S., & Nomikou, P. (2018). Distribution of fine-grained tephra from the 1650 CE submarine eruption of Kolumbo volcano, Greece. *Journal of Volcanology and Geothermal Research*, 352, 10-25, <https://doi.org/10.1016/j.jvolgeores.2018.01.004>
- Giba, M., Walsh, J. J., Nicol, A., Mouslopoulou, V., & Seebeck, H. (2013). Investigation of the spatio-temporal relationship between normal faulting and arc volcanism on million-year time scales. *Journal of the Geological Society*, 170(6), 951-962, <https://doi.org/10.1144/jgs2012-121>
- Hill, D. P., Pollitz, F., & Newhall, C. (2002). Earthquake-volcano interactions. *Physics Today*, 55(11), 41-47, <https://doi.org/10.1063/1.1535006>
- Hübscher, C., Hensch, M., Dahm, T., Dehghani, A., Dimitriadis, I., Hort, M., & Taymaz, T. (2006). Toward a risk assessment of central Aegean volcanoes. *Eos, Transactions American Geophysical Union*, 87(39), 401-407, <https://doi.org/10.1029/2006EO390002>
- Hübscher, C., Ruhnu, M., & Nomikou, P. (2015). Volcano-tectonic evolution of the polygenetic Kolumbo submarine volcano/Santorini (Aegean Sea). *Journal of Volcanology and Geothermal Research*, 291, 101-111, <https://doi.org/10.1016/j.jvolgeores.2014.12.020>
- Hooft, E. E., Nomikou, P., Toomey, D. R., Lampridou, D., Getz, C., Christopoulou, M. E., ... & Van der Beek, B. P. (2017). Backarc tectonism, volcanism, and mass wasting shape seafloor morphology in the Santorini-Christiana-Amorgos region of the Hellenic Volcanic Arc. *Tectonophysics*, 712, 396-414, <https://doi.org/10.1016/j.tecto.2017.06.005>
- Jackson, C. A. L. (2012). Seismic reflection imaging and controls on the preservation of ancient sill-fed magmatic vents. *Journal of the Geological Society*, 169(5), 503-506, <https://doi.org/10.1144/0016-76492011-147>
- Karstens, J., Crutchley, G., Elger, J., Kühn, M., Schmid, F., Dalla Valle, G., ... & Nomikou, P. (2020). R/V Poseidon Cruise Report 538-THESEUS Tsunami hazard of explosive submarine eruptions, 15th July–26th July, 2019 Cartagena (Spain)-Heraklion (Greece), <http://oceanrep.geomar.de/id/eprint/49501>
- Karstens, J., Crutchley, G. J., Hansteen, T., Preine, J., Carey, S., Elger, J.,

Kühn, M., Nomikou, P., Schmid, Fl., Dalla Valle, G., Kelfoun, K., Berndt, C. Set up to fail – cascading events during the 1650 tsunamigenic eruption of Kolumbo volcano. In Review_A, Nature Communications

Karstens, J., \Preine, J., Crutchley, G. J., Kutterolf, S., van der Bilt, W. G. M., Hooft, E. E. E., Druitt, T. H., Schmid, F., Cederstr\o m, J. M., Hübscher, C., Nomikou, P., Carey, S., Kühn, M., Elger, J., Berndt, C. Revised Minoan eruption volume as benchmark for large volcanic eruptions. In Review_B, Nature Communications.

Klaver, M., Carey, S., Nomikou, P., Smet, I., Godelitsas, A., & Vroon, P. (2016). A distinct source and differentiation history for Kolumbo submarine volcano, Santorini volcanic field, Aegean arc. *Geochemistry, Geophysics, Geosystems*, 17(8), 3254-3273, <https://doi.org/10.1002/2016GC006398>

Lynett, P., McCann, M., Zhou, Z., Renteria, W., Borrero, J., Greer, D., ... & Cinar, G. E. (2022). Diverse tsunamigenesis triggered by the Hunga Tonga-Hunga Ha’apai eruption. *Nature*, 609(7928), 728-733, <https://doi.org/10.1038/s41586-022-05170-6>

Magee, C., Hunt-Stewart, E., & Jackson, C. A. L. (2013). Volcano growth mechanisms and the role of sub-volcanic intrusions: Insights from 2D seismic reflection data. *Earth and Planetary Science Letters*, 373, 41-53, <https://doi.org/10.1016/j.epsl.2013.04.041>

Magee, C., Muirhead, J. D., Karvelas, A., Holford, S. P., Jackson, C. A., Bastow, I. D., ... & Shtukert, O. (2016). Lateral magma flow in mafic sill complexes. *Geosphere*, 12(3), 809-841 <https://doi.org/10.1130/GES01256.1>

McVey, B. G., Hooft, E. E. E., Heath, B. A., Toomey, D. R., Paulatto, M., Morgan, J. V., ... & Papazachos, C. B. (2020). Magma accumulation beneath Santorini volcano, Greece, from P-wave tomography. *Geology*, 48(3), 231-235, <https://doi.org/10.1130/G47127.1>

Mitchell, N. (2012). Hot, cracking rocks deep down. *Nature Geoscience*, 5(7), 444-445, <https://doi.org/10.1038/ngeo1505>

Nomikou, P., Carey, S., Papanikolaou, D., Bell, K. C., Sakellariou, D., Alexandri, M., & Bejelou, K. (2012). Submarine volcanoes of the Kolumbo volcanic zone NE of Santorini Caldera, Greece. *Global and Planetary Change*, 90, 135-151., <https://doi.org/10.1016/j.gloplacha.2012.01.001>

Nomikou, P., Papanikolaou, D., Alexandri, M., Sakellariou, D., & Rousakis, G. (2013). Submarine volcanoes along the Aegean volcanic arc. *Tectonophysics*, 597, 123-146, <https://doi.org/10.1016/j.tecto.2012.10.001>

Nomikou, P., Druitt, T. H., Hübscher, C., Mather, T. A., Paulatto, M., Kalnins, L. M., ... & Parks, M. M. (2016a). Post-eruptive flooding of Santorini caldera and implications for tsunami generation. *Nature communications*, 7(1), 1-10, <https://doi.org/10.1038/ncomms13332>

- Nomikou, P., Hübscher, C., Ruhнау, M., & Bejelou, K. (2016b). Tectonostratigraphic evolution through successive extensional events of the Anydros Basin, hosting Kolumbo volcanic field at the Aegean Sea, Greece. *Tectonophysics*, 671, 202-217, <https://doi.org/10.1016/j.tecto.2016.01.021>
- Nomikou, P., Hübscher, C., Papanikolaou, D., Farangitakis, G. P., Ruhнау, M., & Lampridou, D. (2018a). Expanding extension, subsidence and lateral segmentation within the Santorini-Amorgos basins during Quaternary: Implications for the 1956 Amorgos events, central-south Aegean Sea, Greece. *Tectonophysics*, 722, 138-153, <https://doi.org/10.1016/j.tecto.2017.10.016>
- Nomikou, P., Hübscher, C., & Carey, S. (2019). The Christiana-Santorini-Kolumbo Volcanic Field. *Elements: An International Magazine of Mineralogy, Geochemistry, and Petrology*, 15(3), 171-176, <https://doi.org/10.2138/gselements.15.3.171>
- Planke, S., Rasmussen, T., Rey, S. S., & Myklebust, R. (2005, January). Seismic characteristics and distribution of volcanic intrusions and hydrothermal vent complexes in the Vøring and Møre basins. In *Geological Society, London, Petroleum Geology Conference series* (Vol. 6, No. 1, pp. 833-844). Geological Society of London, <https://doi.org/10.1144/0060833>
- Paulatto, M., Hooft, E., Chrapkiewicz, K., Heath, B., Toomey, D., & Morgan, J. (2022). Advances in seismic imaging of magma and crystal mush, <https://doi.org/10.31223/X5CS8S>
- Pope, E. L., Jutzeler, M., Cartigny, M. J., Shreeve, J., Talling, P. J., Wright, I. C., & Wysoczanski, R. J. (2018). Origin of spectacular fields of submarine sediment waves around volcanic islands. *Earth and Planetary Science Letters*, 493, 12-24, <https://doi.org/10.1016/j.epsl.2018.04.020>
- Preine, J., Karstens, J., Hübscher, C., Nomikou, P., Schmid, F., Crutchley, G., Papanikolaou, D., Druitt, T. (2022a). Spatio-Temporal Evolution of the Christiana-Santorini-Kolumbo Volcanic Field, Aegean Sea. *Geology*, <https://doi.org/10.1130/G49167.1>
- Preine, J., Karstens, J., Hübscher, C., Crutchley, G. J., Druitt, T. H., Schmid, F., & Nomikou, P. (2022b). The Hidden Giant: How a rift pulse triggered a cascade of sector collapses and voluminous secondary mass-transport events in the early evolution of Santorini. *Basin Research*, <https://doi.org/10.1111/bre.12667>
- Preine, J., Hübscher, C., Karstens, J., & Nomikou, P. (2022c). Volcano-Tectonic Evolution of the Christiana-Santorini-Kolumbo Rift Zone. *Tectonics*, <https://doi.org/10.1029/2022TC007524>
- Reynolds, P., Schofield, N., Brown, R. J., & Holford, S. P. (2018). The architecture of submarine monogenetic volcanoes—insights from 3D seismic data. *Basin Research*, 30, 437-451, <https://doi.org/10.1111/bre.12230>
- Rizzo, A. L., Caracausi, A., Chavagnac, V., Nomikou, P., Polymenakou, P. N., Mandalakis, M., ... & Lampridou, D. (2016). Kolumbo submarine volcano

(Greece): An active window into the Aegean subduction system. *Scientific reports*, 6(1), 1-9, <https://doi.org/10.1038/srep28013>

Schmid, F., Petersen, G., Hooft, E., Paulatto, M., Chrapkiewicz, K., Hensch, M., & Dahm, T. (2022). Heralds of Future Volcanism: Swarms of Microseismicity Beneath the Submarine Kolumbo Volcano Indicate Opening of Near-Vertical Fractures Exploited by Ascending Melts. *Geochemistry, Geophysics, Geosystems*, 23(7), <https://doi.org/10.1029/2022GC010420>

Sigurðsson, H., Carey, S., Alexandri, M., Vougioukalakis, G., Croff, K., Roman, C., ... & Nomikou, P. (2006). Marine investigations of Greece's Santorini volcanic field. *Eos, Transactions American Geophysical Union*, 87(34), 337-342, <https://doi.org/10.1029/2006EO340001>

Sun, Q., Magee, C., Jackson, C. A. L., Mitchell, S. J., & Xie, X. (2020). How do deep-water volcanoes grow?. *Earth and Planetary Science Letters*, 542, 116320, <https://doi.org/10.1016/j.epsl.2020.116320>

Taner, M. T., Koehler, F., & Sheriff, R. E. (1979). Complex seismic trace analysis. *Geophysics*, 44(6), 1041-1063, <https://doi.org/10.1190/1.1440994>

Tibaldi, A. (1995). Morphology of pyroclastic cones and tectonics. *Journal of Geophysical Research: Solid Earth*, 100(B12), 24521-24535, <https://doi.org/10.1029/95JB02250>

Tibaldi, A., Bonali, F. L., Pasquaré, F. A., Rust, D., Cavallo, A., & D'urso, A. (2013). Structure of regional dykes and local cone sheets in the Midhyrna-Lysuskard area, Snaefellsnes Peninsula (NW Iceland). *Bulletin of volcanology*, 75(11), 1-16, <https://doi.org/10.1007/s00445-013-0764-8>

Tibaldi, A., & Bonali, F. L. (2017). Intra-arc and back-arc volcano-tectonics: Magma pathways at Holocene Alaska-Aleutian volcanoes. *Earth-Science Reviews*, 167, 1-26, <https://doi.org/10.1016/j.earscirev.2017.02.004>

Vakhrameeva, P., Koutsodendris, A., Wulf, S., Fletcher, W. J., Appelt, O., Knipping, M., ... & Pross, J. (2018). The cryptotephra record of the Marine Isotope Stage 12 to 10 interval (460–335 ka) at Tenaghi Philippon, Greece: Exploring chronological markers for the Middle Pleistocene of the Mediterranean region. *Quaternary Science Reviews*, 200, 313-333, <https://doi.org/10.1016/j.quascirev.2018.09.019>

Vakhrameeva, P., Wulf, S., Koutsodendris, A., Tjallingii, R., Fletcher, W. J., Appelt, O., ... & Pross, J. (2019). Eastern Mediterranean volcanism during marine isotope stages 9 to 7e (335–235 ka): insights based on cryptotephra layers at Tenaghi Philippon, Greece. *Journal of Volcanology and Geothermal Research*, 380, 31-47, <https://doi.org/10.1016/j.jvolgeores.2019.05.016>

Figure captions

Figure 1: (a) Regional map of the southern Aegean Sea showing the Hellenic Volcanic Arc (shaded red) with volcanic centers marked

by red triangles. The coordinate system here (and in subsequent maps) is UTM Zone 35N, WGS84 datum. The red box indicates the study area shown in (b). (b) Morphological map of the CSK rift zone showing islands, basins, volcanic centers, and major extensional structures (red lines), after Nomikou et al. (2016b, 2018a, 2019) and Preine et al. (2022b). Grey lines indicate all available seismic profiles. KaL: Kameni Line; KoL: Kolumbo Line (after Heath et al., 2019). Bathymetry from Nomikou et al. (2012, 2013, 2018a, 2019) and Hooft et al. (2017). (c) Close-up of the western Anhydros Basin showing the KVC and major structural elements. Color scale same as (b). (d) Profile curvature from the bathymetric map shown in c. Volcanic cones are labeled according to Nomikou et al. (2012) and Hooft et al. (2017). Asterisks indicate cones with summit craters. A northeast-trending ridge identified in this study is labeled “Kolumbo Ridge”. Orange lines indicate the two main trends of the KVC (Nomikou et al., 2012).

Figure 2: (a) NW-SE oriented seismic profile HH06-22 crossing the Anhydros Basin and Kolumbo. KF: Kolumbo Fault. (b) SW-NE oriented seismic profile UHH06-35 crossing Kolumbo and several cones of the KVC. Orange triangles mark onlap terminations. Colored horizons h1-h6 mark key reflections separating seismostratigraphic units U1-U6 from Preine et al. (2022a). K1-K5: Kolumbo Units after Hübscher et al. (2015). VC: volcanic cone. KF: Kolumbo Fault. Inset map is an extract from Figure 1c, showing the locations of the profiles in (a) and (b). See Figure S2 for an uninterpreted version of the seismic profiles.

Figure 3: (a) Seismic profile UHH06-24 crossing the Anhydros Basin and the southwestern part of the KVC. (b) Seismic profile UHH06-25 crossing the Anhydros Basin and the central part of the KVC. (c) Seismic profile UHH06-02 across the Ios shelf, the Anhydros Basin, and the central part of the KVC. Inset map is an extract from Figure 1c, showing the locations of the profiles in (a) - (c). See Figure S3 for an uninterpreted version of the seismic profiles.

Figure 4: (a-f) Detailed illustration of the internal architecture of several cones of the KVC. Left panels show seismic amplitude and right panels show instantaneous phase. SF1, SF2: Seismic facies as explained in the text; HAR: High-Amplitude reflection. See Figure S4 for an uninterpreted version of the seismic profiles.

Figure 5: Seismic profiles across the northeastern KVC and the eastern Anhydros Basin (a-e). Profiles in (b) and (c) are single-channel seismic profiles, in which the yellow arrows indicate the position of the bubble reflection (acquisition artefact). Prominent faults Ab1-Ab3 are highlighted and their location is indicated in the map (f). IF: Ios Fault; AhF: Anhydros Fault. See Figure S5 for an uninterpreted

version of the seismic profiles.

Figure 6: (a) Seismic profile UHH06-29 traversing the northeast flank of Santorini, Kolumbo, and the Anhydros Horst. (b) Seismic profile UHH06-19 crossing the Anhydros Basin and the Kolumbo Ridge between Santorini and Kolumbo. (c) Seismic profile UHH06-38 crossing the northeastern flank of Santorini. Inset map show the locations of the seismic lines in (a)-(c). See Figure S6 for an uninterpreted version of the seismic profiles.

Figure 7: (a) Relative timeline of the evolution of the CSK volcanic field, placed in the context of the chronostratigraphic framework of Preine et al. (2022a) – i.e. horizons h3 – h6. Ch.: Christiana, TPF: Thera Pyroclastic Formation, LBA: Late Bronze Age eruption, VC = volcanic cone, OC = Oia Cone. Black arrows indicate increasing age from one volcanic cone to the next. (b) Map of profile curvature showing the direction of onlap terminations from individual cones inferred from the seismic lines. (c) Schematic diagram showing the interpreted internal architecture of exemplary volcanic edifices of the KVC. The approximate location of the sketched section is indicated by the dashed black line in (b). SF: Seismic facies, HAR: High-Amplitude reflection.

Figure 8: (a) Morphological map of the CSK rift zone showing major volcano-tectonic features before the onset of the Thera Pyroclastic Formation (TPF, ~ 0.3 Ma). Outline of proto-Anhydros Basin taken from Heath et al. (2019) and Preine et al. (2022c). Previously identified faults from Nomikou et al. (2019) and Preine et al. (2022c). Kameni and Kolumbo Lines according to Heath et al. (2019). Low-Velocity Volume zone from McVey et al. (2019). Locations of cones from Phases 1-3 taken from Preine et al. (2022a) and from this study. Locations of sampled lava outcrops from Pank et al. (2022). (c-e) Sketches of the spatio-temporal evolution of the Kolumbo Volcanic Cones (KVC) in the context of the entire Christiana-Santorini-Kolumbo volcanic field (according to Preine et al., 2022a). Red semi-transparent color indicates the approximate area of volcanic activity during each phase. Fault evolution according to Preine et al. (2022c). Present-day coastlines for spatial reference.

Spatio-temporal evolution of the Kolumbo Volcanic Chain and its link to the volcanic plumbing system of Santorini

J. Preine¹, C. Hübscher¹, J. Karstens², G. J. Crutchley², P. Nomikou³

¹University of Hamburg, Institute of Geophysics, Hamburg, Germany

²GEOMAR – Helmholtz Zentrum für Ozeanforschung, Marine Geophysics, Kiel, Germany

³National and Kapodistrian University of Athens, Athens, Greece

Contents of this file

Text S1
Figure S2
Figure S3
Figure S4
Figure S5
Figure S6

Introduction

Here we present supporting information for the paper titled "Spatio-temporal evolution of the Kolumbo Volcanic Chain and its link to the volcanic plumbing system of Santorini". Contained in this file is a description of the processing of the seismic reflection data (Text S1), and uninterpreted versions of the seismic profiles shown in Figures 2-6 (Figure S2-S6).

Text S1.

The seismic data used in this study are from two cruises between from 2006 (Sigurdsson et al., 2006; Hübscher et al., 2006). Single-channel seismic data were acquired in 2006 during the THERA project on RV Aegaeo. As the seismic source, a G-pulser was used with a volume of 10 in³. The general processing comprised simple bandpass filtering (15-500 Hz), de-spiking, and spherical divergence correction. In order to migrate the data, we binned the shot points into a regular spacing of 10 m. After migration, we applied a top-mute and white-noise removal. The vertical resolution of these data can be approximated to 8-15 m (using the $\lambda/4$ - or $\lambda/2$ -approximation) within the shallow sediments ($v=1900$ m/s).

For the cruise POS338 with RV Poseidon, a GI-pulser was used and operated in true GI mode with a primary (Generator) volume of 45 in³ and a secondary (Injector) volume of 105 in³. Using a 600 m analog streamer with 24 Channels, we defined a CMP-spacing of 12.5 m. Processing of these data comprised trace-editing, simple frequency filtering (10-500 Hz), suppression of a receiver-ghost signal by predictive deconvolution, surface-related multiple elimination as well as spherical divergence correction, pre-stack time migration followed by top-muting and white-noise removal. These data have a main frequency of 60 Hz indicating a vertical resolution of approx. 8-15 m.

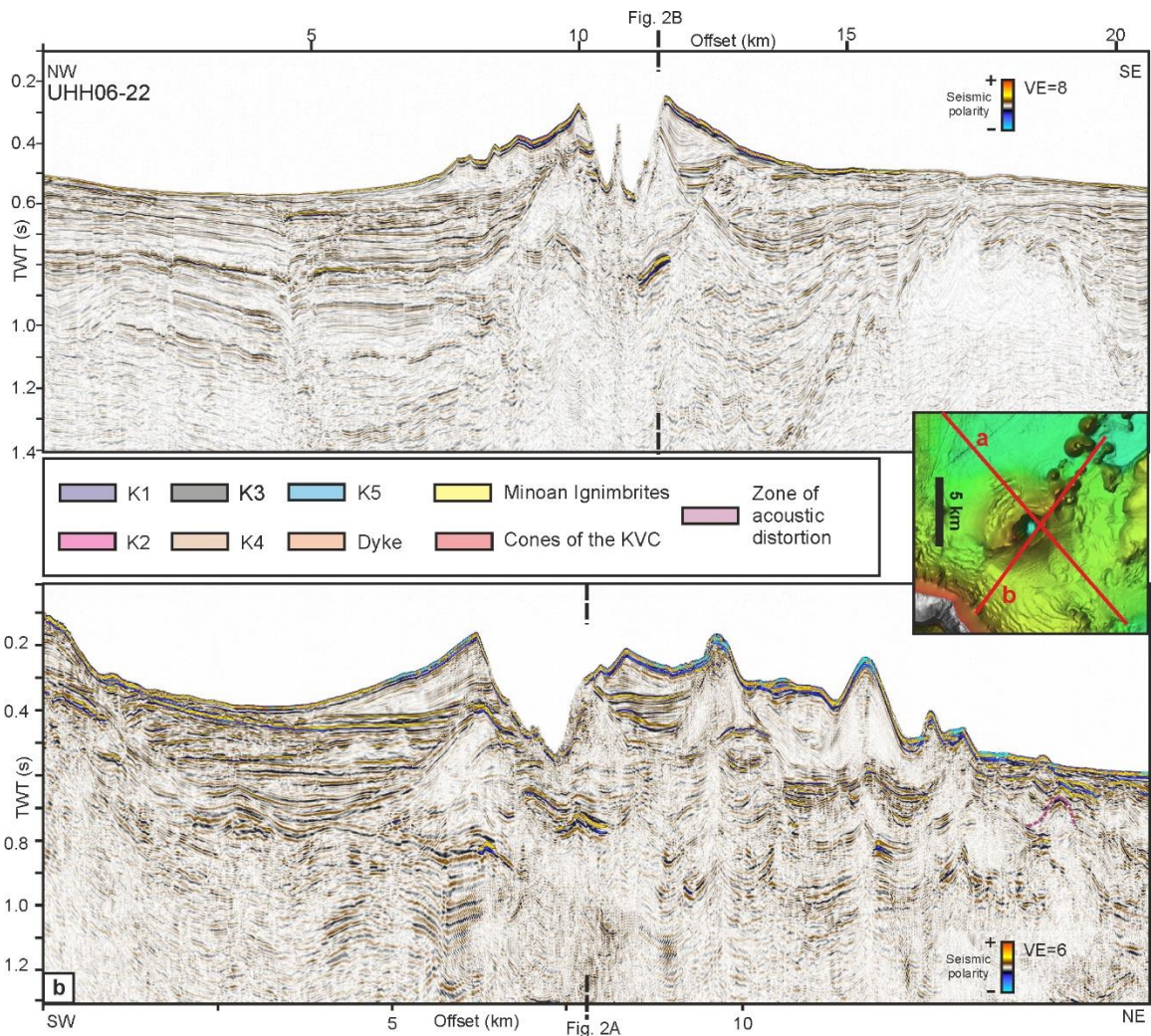


Figure S2. Uninterpreted version of the seismic profiles shown in Figure 2.

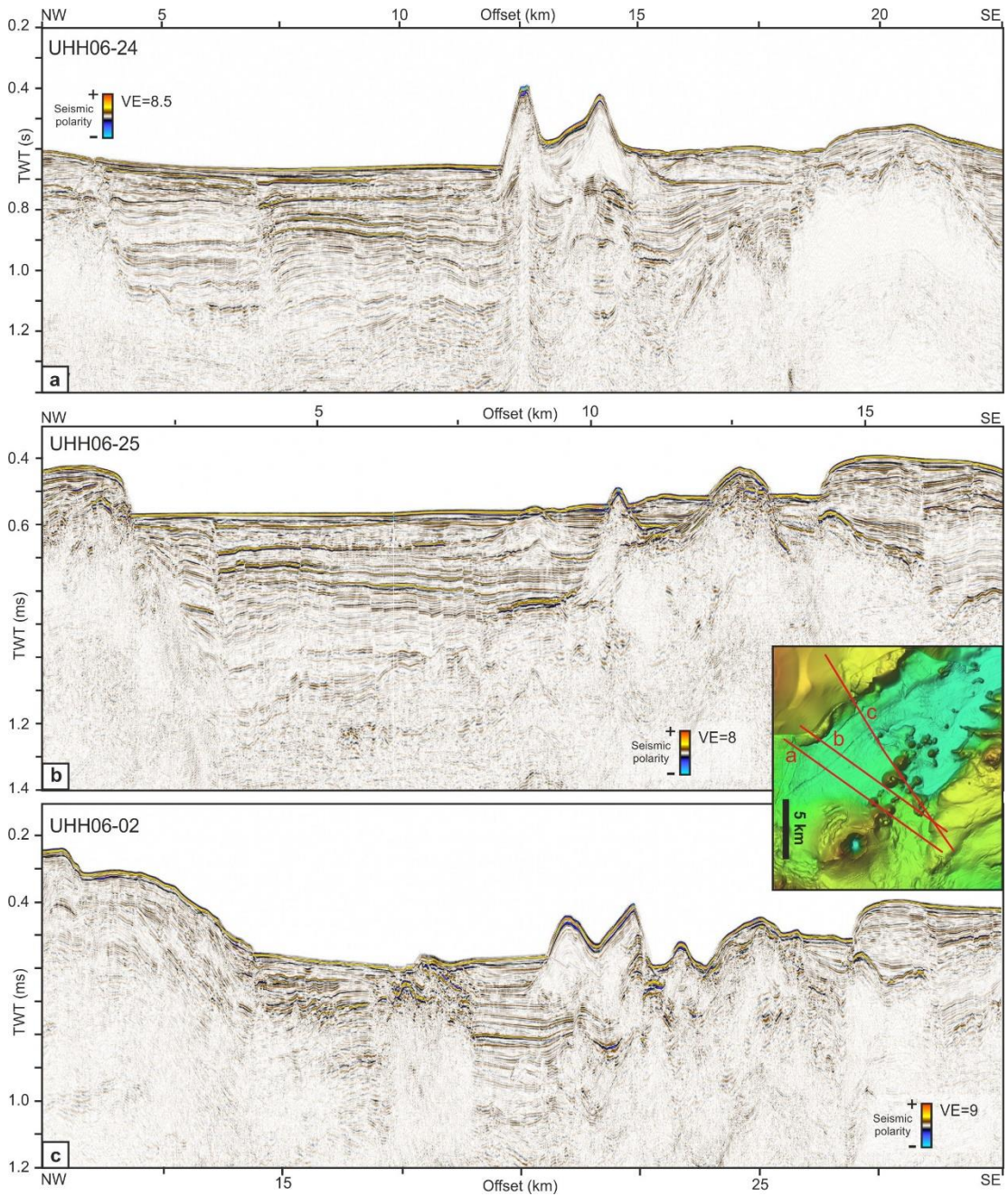


Figure S3. Uninterpreted version of the seismic profiles shown in Figure 3.

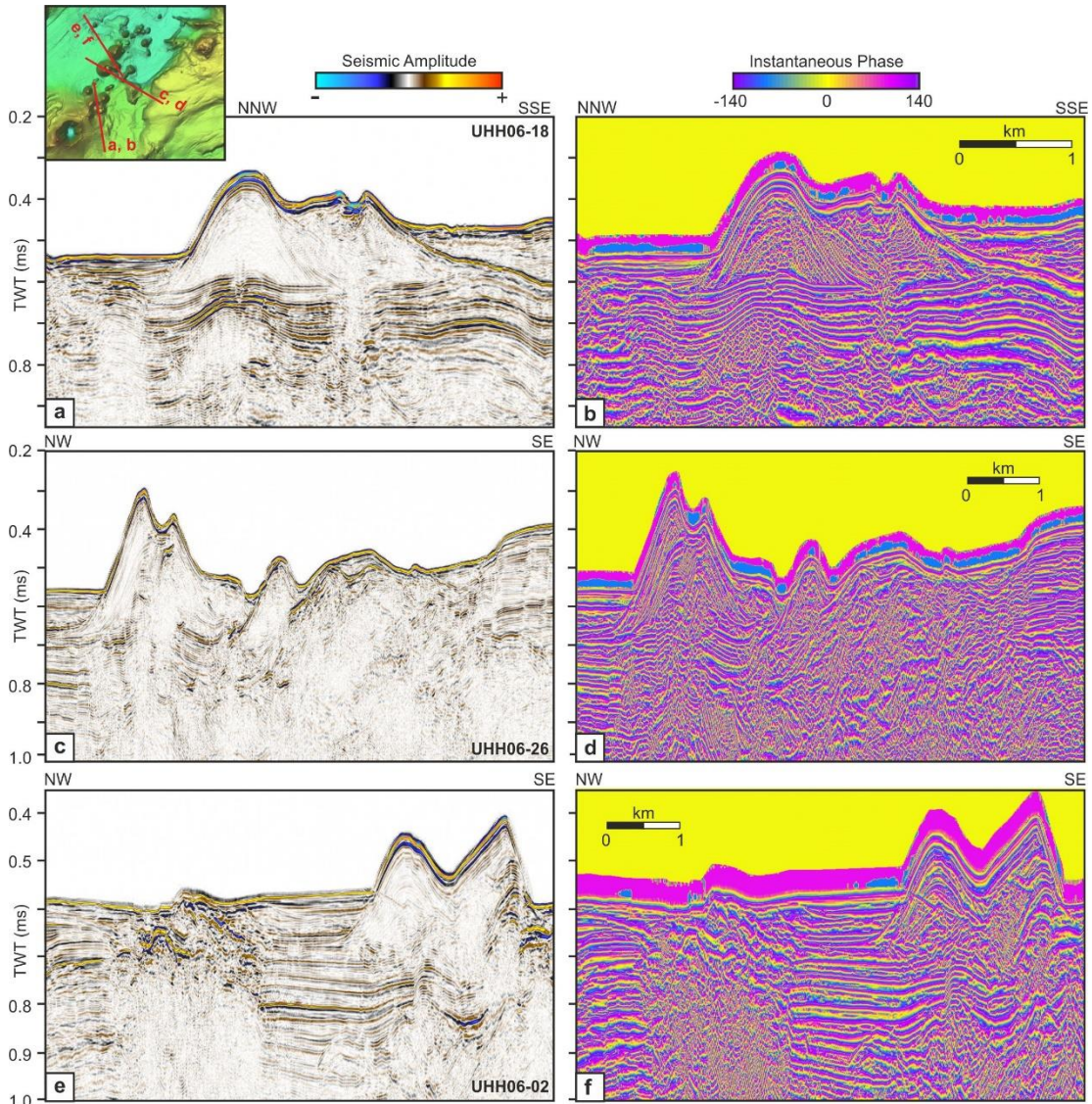


Figure S4. Uninterpreted version of the seismic profiles shown in Figure 4.

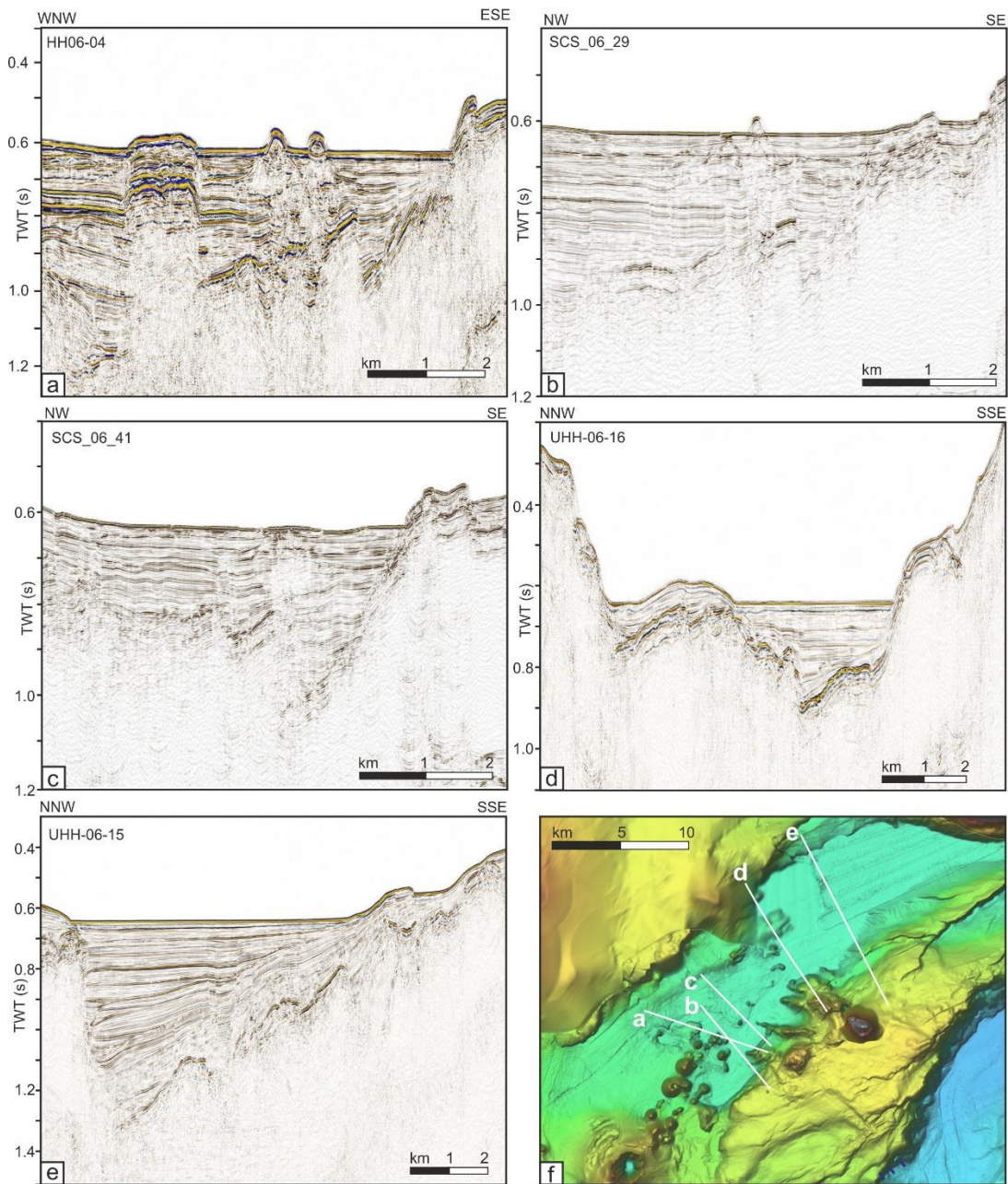


Figure S5. Uninterpreted version of the seismic profiles shown in Figure 5.

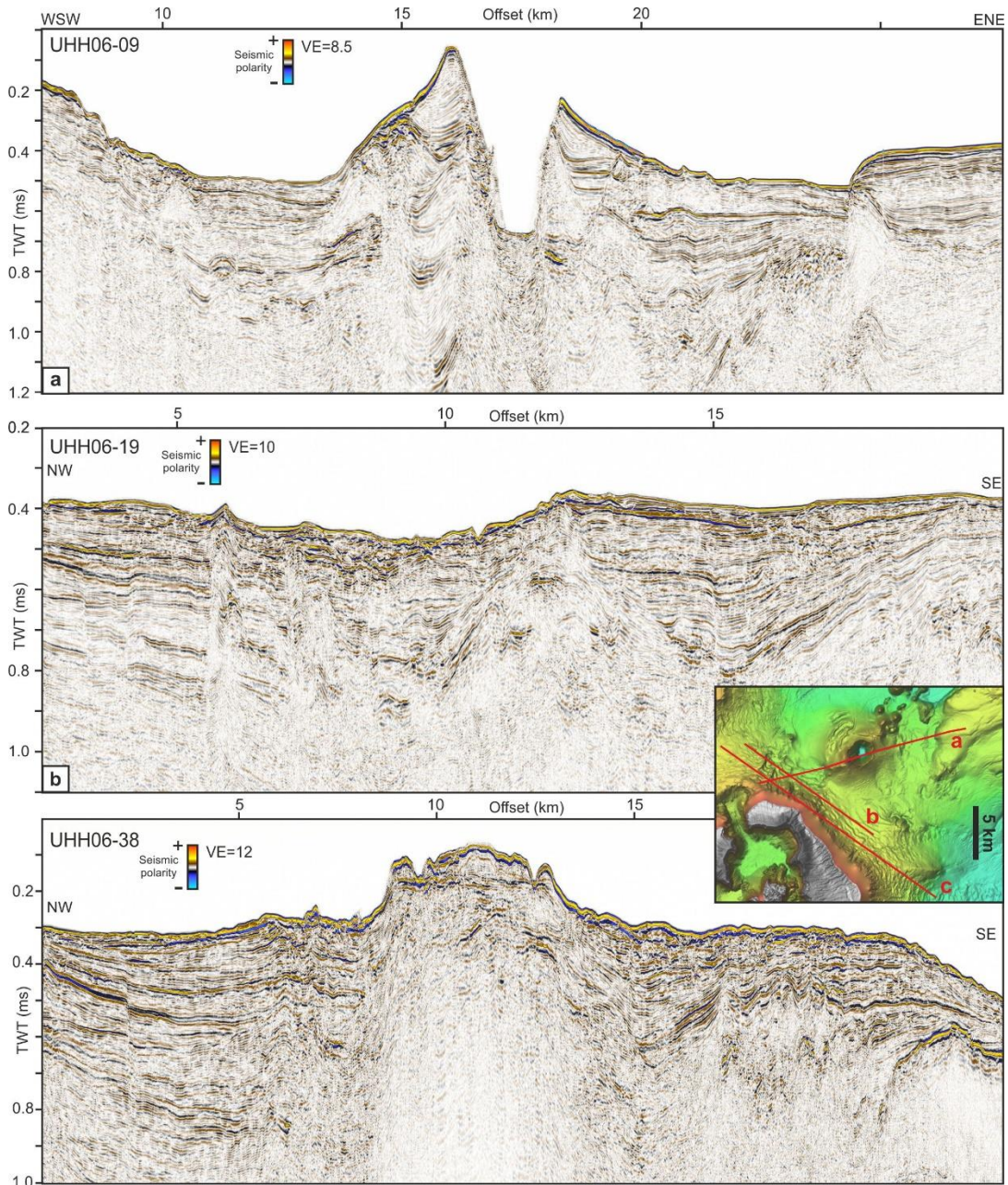


Figure S6. Uninterpreted version of the seismic profiles shown in Figure 6.